JPEDAV (2009) 30:571–576
DOI: 10.1007/s11669-009-9567-1
1547-7037 ©ASM International

Integrating CALPHAD into Phase Field Simulations for Practical Applications

Kaisheng Wu, Shuanglin Chen, Fan Zhang, and Y.A. Chang

(Submitted April 15, 2009; in revised form July 2, 2009)

Phase field modeling is a powerful tool for simulations of the microstructure evolutions. Its applications to practical alloy systems, however, have been limited mostly due to difficulties in relating the energy functional to the thermodynamic properties of the systems and mobilities to kinetic properties of the alloy elements involved. A phase field modeling tool, PanROME (Research Of Microstructure Evolution), has been developed that offers capabilities to overcome these difficulties. It can use the thermodynamic and kinetic databases that are built based on the CALPHAD approach, thus making it suitable for simulations in multicomponent and multiphase systems. This phase field model integrates Kim-Kim-Suzuki (KKS) model which allows simulations in a practical length scale while maintaining a reasonable interfacial energy with a multiphase model that is applicable to multiphase systems. Several applications of the PanROME modeling tool to Ni-base superalloys are demonstrated in the present article.

Keywords CALPHAD, computational studies, diffusion, microstructure, Ni-base superalloys, phase field modeling, phase transformation

1. Introduction

The phase field method has advanced rapidly in recent years due to its power and flexibility in revealing the governing mechanisms of various phase transformations and in simulating complex systems with multiple mechanisms involved. It treats the interface between two different phase states as a diffused, gradient region, which remarkably simplifies numerical treatment since it is not necessary to track the interface position, and can thus be easily applied to complicated pattern evolutions. Moreover, it conveniently incorporates various driving forces such as chemical, stress, and magnetic contributions so that it can simulate a wide range of phenomena such as alloy solidification,[1-3] solid-state transformation,[4-6] grain growth,[7-10] and dislocation dynamics.[11-13]

Applications of the phase field method to practical multicomponent and multiphase systems are, however, still quite limited. One of the major obstacles is that most existing models lack the capability, fundamentally or numerically, to construct the free energy functional directly from real-phase diagrams and thermochemical data. Kim, Kim and Suzuki (KKS) proposed a model that can be applied to multicomponent systems and has the potential to use the real-phase diagrams data[14-16] (“real phase diagrams” means that they are not the prototype systems that the phase field method initially used). The most attractive advantage of the KKS model is much less restriction on the interface thickness than other formulations. This advantage makes it suitable for applications in a practical length scale, but the original version is limited to two-phase systems, and the computational cost is greatly increased. The multiphase concept for phase field modeling is rationalized by Steinbach et al.,[3,17] though the relationship between the potential free energy and real thermodynamic properties is not straightforward.

The current study aims to develop a phase field tool to circumvent these difficulties by coupling the KKS model with a multiphase model. The tool, named PanROME (Research Of Microstructure Evolution), directly utilizes CALPHAD-type databases to obtain the thermodynamic and kinetic properties of arbitrary alloy systems. It develops a free energy functional that combines the advantages of the KKS model and a multiphase model. A sophisticated algorithm similar to that used in phase diagram calculations is designed to greatly improve the computational efficiency. These efforts will expedite the practical applications of phase field modeling to meet the increasing demands of computational tools for complicated microstructure evolutions in multicomponent and multiphase systems.

This article is an invited paper selected from participants of the 14th National Conference and Multilateral Symposium on Phase Diagrams and Materials Design in honor of Prof. Zhanpeng Jin’s 70th birthday, held November 3-5, 2008, in Changsha, China. The conference was organized by the Phase Diagrams Committee of the Chinese Physical Society with Drs. Huashan Liu and Libin Liu as the key organizers. Publication in *Journal of Phase Equilibria and Diffusion* was organized by J.-C. Zhao, The Ohio State University; Yong Du, Central South University; and Qing Chen, Thermo-Calc Software AB.

Kaisheng Wu, Shuanglin Chen, and **Fan Zhang**, CompuTherm LLC, 437 S. Yellowstone Dr. Suite 217, Madison, WI 53719; **Y.A. Chang**, Department of Materials Science and Engineering, University of Wisconsin-Madison, 1509 University Ave., Madison, WI 53706. Contact e-mail: kaisheng.wu@computherm.com.

2. Model Formulation

2.1 Free Energy Formulation

Following Steinbach et al.,[17] we describe a system with $n + 1$ components and m phases by a set of n conserved variables, $X = (X_1, X_2, \ldots, X_k, \ldots, X_n)$, and m non-conserved variables, $\phi = (\phi_1, \phi_2, \ldots, \phi_i, \ldots, \phi_m)$. The molar volume of the system V_m is assumed to be constant. X_k represents the concentration (mole fraction) of component k, with $(n + 1)$th component being the solvent whose concentration is not independent

$$X_{n+1} = 1 - \sum_{k=1}^{n} X_k \qquad \text{(Eq 1)}$$

ϕ_i represents phase state i. It takes a non-zero value only at a single-phase region of phase i, where $\phi_i = 1$, and at a diffused interface between phase i and other phases across the system with a gradual change from 1 to 0.

The free energy functional F of the system can be written as

$$F = \int \left[f(X, \phi) + f^{\text{grad}} \right] dV \qquad \text{(Eq 2)}$$

where $f(X, \phi)$ is the local free energy density which consists of two contributions

$$f(X, \phi) = \frac{g(X, \phi)}{V_m} + f(\phi) \qquad \text{(Eq 3)}$$

where $g(X, \phi)$ is the molar Gibbs free energy and $f(\phi)$ is the free energy penalty originated from the coexistence of different phases. $g(X, \phi)$ is constructed using the KKS model[14-16] and can be defined as

$$g(X, \phi) = \sum_{i=1}^{m} h(\phi_i) g^i(X^i) \qquad \text{(Eq 4)}$$

$h(\phi_i)$ is an arbitrary function which guarantees a change from $h(0) = 0$ to $h(1) = 1$. To facilitate programming we define

$$h(\phi_i) = \phi_i, \quad i = 1, \ldots, m \qquad \text{(Eq 5)}$$

$g^i(X^i)$ in Eq 4 is the molar Gibbs free energy of phase i. $X^i = (X_1^i, X_2^i, \ldots, X_k^i, \ldots, X_n^i)$ represents concentration in phase i. It is obtained by constraints of mixture rule as well as equal chemical potential condition

$$X_k = \sum_{i=1}^{m} h(\phi_i) X_k^i \quad k = 1, 2, \ldots, n \qquad \text{(Eq 6)}$$

$$\frac{\partial g^1}{\partial X_k^1} = \frac{\partial g^2}{\partial X_k^2} = \cdots = \frac{\partial g^i}{\partial X_k^i} = \cdots = \frac{\partial g^m}{\partial X_k^m} \equiv \tilde{\mu}_k \quad k = 1, 2, \ldots, n \qquad \text{(Eq 7)}$$

$f(\phi)$ in Eq 3 is defined as

$$f(\phi) = \sum_{i=1}^{m} \sum_{j>i}^{m} \omega_{ij} \phi_i^2 \phi_j^2 \qquad \text{(Eq 8)}$$

where ω_{ij} is the energy barrier between phases i and j.

The gradient energy term f^{grad} in Eq 2 is dependent explicitly only on phase variables ϕ[17]

$$f^{\text{grad}} = \sum_{i=1}^{m} \sum_{j>i}^{m} \frac{\epsilon_{ij}}{2} \left(\phi_j \nabla \phi_i - \phi_i \nabla \phi_j \right)^2 \qquad \text{(Eq 9)}$$

where ϵ_{ij} is the gradient coefficient between phases i and j.

2.2 Governing Equations

The time evolution of the conserved variables is governed by the generalized diffusion equation stating the mass conservation condition, usually called Cahn-Hilliard equation[18]

$$\frac{\partial X_k}{\partial t} = V_m^2 \nabla \cdot \tilde{M}_{kl} \sum_{l=1}^{n} \nabla \frac{\delta F}{\delta X_l} \qquad \text{(Eq 10)}$$

Based on Eq 2-7 it can be rewritten as (for detailed derivation of $\frac{\delta F}{\delta X_l}$ please see Ref 16)

$$\frac{\partial X_k}{\partial t} = V_m \nabla \cdot \tilde{M}_{kl} \sum_{l=1}^{n} \nabla \tilde{\mu}_l \qquad \text{(Eq 11)}$$

with $\tilde{\mu}_l$ being defined in Eq 7. $\tilde{M}_{kl}$ is the chemical mobility which can be related to the atomic mobilities B_p as (when molar volume is constant)[19]

$$\tilde{M}_{kl} = \frac{1}{V_m} \sum_{p=1}^{n} \left(\delta_{kp} - X_k \right) \left(\delta_{lp} - X_l \right) X_p B_p \qquad \text{(Eq 12)}$$

we further assume that B_p follows rule of mixture

$$B_p = \sum_{i=1}^{m} h(\phi_i) B_p^i \quad p = 1, 2, \ldots, n \qquad \text{(Eq 13)}$$

where B_p^i is the atomic mobility of component p in the structure of phase i.

The temporal evolution of non-conserved variables is governed by[20,21]

$$\frac{\partial \phi_i}{\partial t} = -L_i \frac{\delta F}{\delta \phi_i} \quad i = 1, 2, \ldots, m \qquad \text{(Eq 14)}$$

where L_i is a positive parameter characterizing interface mobility. From Eq 4, 8-9 the variance of free energy with respect to ϕ_i can be obtained as[14-17]

$$\frac{\delta F}{\delta \phi_i} = \frac{1}{V_m} \left\{ g^i(X^i) - \sum_{j=1, j \neq i}^{m} \left[g^j(X^j) + \sum_{k=1}^{n} \left(X_k^i - X_k^j \right) \tilde{\mu}_k \right] \right\} + 2\phi_i \sum_{j=1, j \neq i}^{m} \omega_{ij} \left(\phi_j^2 - \phi_i \phi_j \right) - \sum_{j=1, j \neq i}^{m} \epsilon_{ij} \left(\phi_j \nabla^2 \phi_i - \phi_i \nabla^2 \phi_j \right) \qquad \text{(Eq 15)}$$

2.3 Coupling with CALPHAD Databases and Physical Parameters

The model is able to utilize thermodynamic and kinetic databases that are established by means of the *CALPHAD*

technique.[22] Thermodynamic databases provide the Gibbs free energy of individual phases ($g^i(X^i)$ in Eq 4) while kinetic databases provide atomic mobilities of components in various phases[23,24] (B_p^i in Eq 13).

The interfacial energy, σ_{ij}, between phases i and j is related to model parameters[15]

$$\sigma_{ij} = \frac{\epsilon_{ij}\sqrt{\omega_{ij}}}{3\sqrt{2}} \quad \text{(Eq 16)}$$

with ϵ_{ij} and ω_{ij} being defined in Eq 9 and 8, respectively.

The kinetic parameter L_i in Eq 14 is related to different physical parameters depending on the microstructural features the phase field model describes. For example, in alloy solidifications it is related to interface velocity, the latent heat of fusion, the melting temperature as well as the interface thickness.[1] In diffusion-controlled solid-state phase transformations, the interface kinetics is controlled by the Stefan condition which is automatically implemented in Eq 11. L_i, therefore, has no effect as long as it has a sufficiently large value.

3. Numerical Simulation Examples

In this section, several examples in Ni-based superalloys are used to demonstrate the feasibility of the new modeling tool. A CALPHAD database developed in our company, PanNi7,[25] has been used for obtaining thermodynamic and kinetic properties.

3.1 γ + γ′ Diffusion Couple in Ni-Al-Pt System

Recently the γ + γ′ bond coat for gas turbine blade has attracted much attention due to its chemical compatibility with the substrate.[26] Addition of Pt to the bond coat reduces the chemical activity of Al, leading to uphill diffusion of Al from the substrate to the bond coat, and thus increasing the oxidation resistance of the bond coat.[27] Quantitative investigation of the interdiffusion microstructure between the bond coat and substrate is essential to evaluate the lifetime and durability of the bond coat, as well as the property changes of the substrate. For this purpose a series of simulations on the γ + γ′/γ + γ′ diffusion couples in Ni-Al-Pt system have been carried out.

Figure 1 shows a simulation running in a 2D spatial system with 2048×256 grid points. The left half is a γ′ + γ bond coat which has a high amount of Pt with γ′ as the matrix phase. The right half is the γ + γ′ substrate which is initially free from Pt with γ as the matrix phase. As a first approximation the stress effect originated from lattice misfit between γ and γ′ is ignored. The interfacial energy is set to be 0.0114 J/m^2 based on a length scale of 0.3 μm per grid width, which is within the range of the generally acceptable interfacial energy values between γ and γ′. The microstructures are plotted using the Al concentration, with darker shade indicating a higher Al content.

Several significant microstructure changes have been revealed in Fig. 1. Dissolution of the precipitates, γ in the bond coat and γ′ in the substrate, appears at the vicinity of the original boundary (Matano plane), leading to two single-phase layers, γ′ on the bond coat side and γ on the substrate side. The interface between these two layers migrates toward the substrate during the annealing process. Meanwhile, undulation of the interface at an early stage when long-range diffusion is dominant, as shown in Fig. 1(b), decays afterwards when diffusion decreases and capillarity effect plays a more important role on interface curvature, as shown in Fig. 1(c). The newly formed γ layer has a lighter shade than the γ matrix in the substrate, indicating a depletion of Al. These microstructure changes are consistent with the experimental observations.[27] The detailed analyses and quantitative comparisons with experimental data are beyond the scope of this paper and will be published separately.

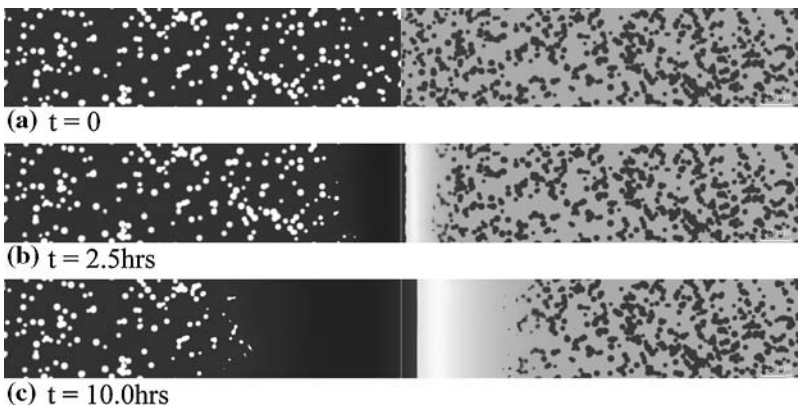

Fig. 1 Simulation of the interdiffusion microstructure evolutions in a Ni-Al-Pt γ′ + γ/γ + γ′ diffusion couple under isothermal annealing at 1200 °C. The initial average composition of the left half (bond coat) is 22 at.% Al, 30 at.% Pt, and 48 at.% Ni with γ′ being the matrix phase (dark background). The initial average composition of the right half (substrate) is 19 at.% Al and 81 at.% Ni with γ being the matrix phase (gray background). System size is 2048×256 grid points. The white vertical line in the middle is the original interface (Matano plane)

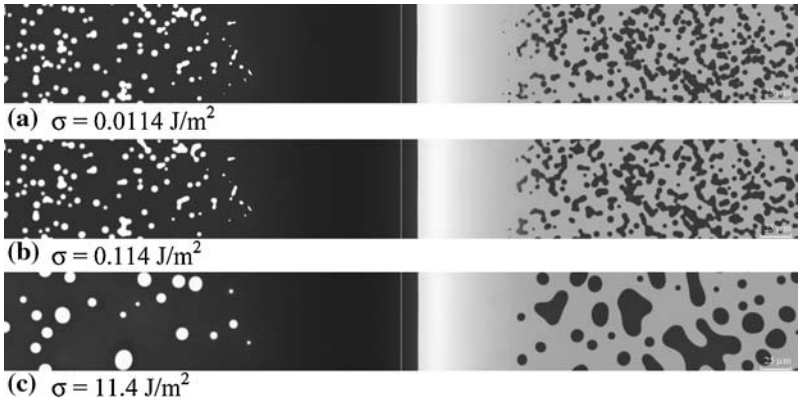

Fig. 2 Comparison of the simulated interdiffusion microstructures varied with the chosen interfacial energies. Simulations are in a Ni-Al-Pt $\gamma' + \gamma/\gamma + \gamma'$ diffusion couple subjected to isothermal annealing at 1200 °C for 10 h. The initial microstructure is shown in Fig. 1(a). The initial average composition of the left half (bond coat) is 22 at.% Al, 30 at.% Pt, and 48 at.% Ni with γ' being the matrix phase (dark background). The initial average composition of the right half (substrate) is 19 at.% Al and 81 at.% Ni with γ being the matrix phase (gray background). System size is 2048×256 grid points. The white vertical line in the middle is the original interface (Matano plane)

Since accurate interfacial energy value from experiments is often unavailable except for a few systems, determination of the interfacial energy in simulations is usually through calibration of the simulated results with corresponding experimental observations such as temporal changes of precipitate sizes. In reality the interfacial energy values between different phases can span a wide range, sometimes even a few orders of magnitude. It is thus important to evaluate the flexibility of the model on the choice of the interfacial energy. The examples shown in Fig. 2 serve this purpose. They start with an identical microstructure as that shown in Fig. 1(a). The interfacial energy employed in Fig. 2(c) is 1000 times larger than that in Fig. 2(a).

It can be seen that these simulations give the same results in terms of the position of the migrated interface, the width of the single-phase layers and the Al depletion zone in the γ layer. The morphology of the remaining precipitates, however, differs significantly. The coalescence and coarsening of the second-phase particles are certainly accelerated by a larger interfacial energy, leading to obviously larger, more isotropic shapes as shown in Fig. 2(c). Precipitates with somewhat elongated shapes can be seen in the cases of smaller interfacial energies, Fig. 2(a) and (b), at the interface between the bond coat and the newly formed γ' layer. This morphology is caused by two interacting processes, the coalescence of neighboring particles driving by reduction of interfacial area, and the dissolution induced by long-range diffusion.

3.2 Co-Coarsening of γ' and β Precipitates in Ni-Al-Cr System

An example of simultaneous coarsening of two precipitate phases is used to examine the feasibility of the model to multiphase systems. The result of $\gamma' + \beta$ co-coarsening in the Ni-Al-Cr system is shown in Fig. 3. Merely for the purpose of demonstrating the feasibility without validation against experiment data for correct interfacial energies, it can be considered as a qualitative test even though thermodynamic and kinetic data for the real Ni-Al-Cr system have been used. In view of this, the real-time scale is undefined and the reduced time τ has been used. The reduced time is defined as $\tau = \frac{BRT}{l^2}t$ where B is the unit of atomic mobility, R is the gas constant, T is the absolute temperature, l is the length scale, and t is the real time. The interfacial energy σ^{i-j} between phase i and j is set as such that

$$\sigma^{\gamma-\beta} = \sigma^{\gamma'-\beta} = 2\sigma^{\gamma-\gamma'} \quad \text{(Eq 17)}$$

The simulation indicates that both phases experience apparent coarsening, while the coarsening rate for β appears to be slightly higher due to its higher interfacial energy. Different from the single-phase ripening process, the morphology as well as coarsening rate is obviously influenced by the surrounding precipitates of different phase states. It is not uncommon that γ' and β particles impinge each other, resulting in an additional energy reduction which replaces one γ-β interface and one γ-γ' interface with one γ'-β interface. This coupled growth or dissolution undoubtedly has an impact on the morphology, size and size distribution of both precipitates. More detailed studies are in progress and will be reported in a separate publication.

4. Discussion

The simulated results demonstrate that the model developed has achieved its design target. The model is deliberately designed to couple two existing models so that we can make fully use of the potential advantages of the phase field method. The KKS model circumvents the direct coupling of interfacial energy with concentration-dependent chemical free energy so that it successfully mitigates the length scale limit when realistic interfacial energy has to be considered.

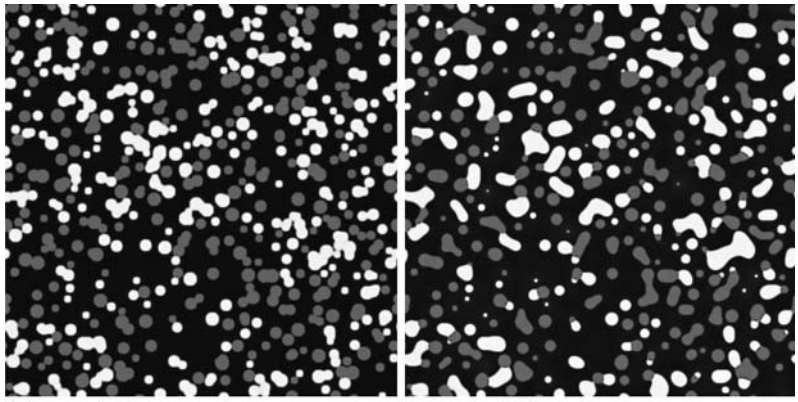

Fig. 3 Qualitative simulation of simultaneous coarsening of γ′ (gray) and β (white) phases in γ matrix (dark background) of Ni-Al-Cr system at 1200 °C. The overall composition of the system is 21.0 at.% Al, 9.0 at.% Cr and 70 at.% Ni. The interfacial energy between γ and β is twice as that between γ and γ′. Numerical size is 512×512 grid points

The multiphase model naturally extends the phase field model, traditionally a two-phase version, to multiphase systems by simply realizing that an interface can be distinguished spatially by two non-conserved field variables. A combination of these two models allows sound treatments of complicated microstructure evolutions in multicomponent and multiphase systems in a practical (mesoscopic) length scale.

Another advantage of the newly developed model is its direct use of CALPHAD databases for important thermodynamic and kinetic inputs. Since so far CALPHAD databases are still the most reliable and comprehensive sources for thermodynamic and kinetic data in practical alloy systems, the model can be readily applied to a variety of industrially important alloys. Meanwhile, least effort is needed to extend the existing model to various processing conditions such as solidification and non-isothermal heat treatments since CALPHAD databases store data that are temperature and composition dependent.

The complexity of the model, especially the part originated from the KKS model, makes it a big challenge with regard to computational affordability. To overcome this difficulty a special algorithm is designed to efficiently solve the KKS model, more specifically Eq 6 and 7. Meanwhile, separating the numerical treatment of the KKS model in the interface region and in the single-phase region also substantially saves the computational time. The current algorithm enables us to perform the simulation examples shown in the previous section using a personal computer with a single core CPU. More complex microstructure and 3D simulations increase the computational time substantially and parallel algorithms have been seeking to meet this demand.

5. Conclusion

A phase field model is developed which allows for efficient description of microstructure evolutions in multicomponent and multiphase systems and it can also treat stoichiometric phases as long as at least one phase is solution phase. It directly utilizes CALPHAD databases for accurate thermodynamic and kinetic parameters. Simulations at a practical (mesoscopic) length scale have been achieved at a tolerable computational cost. Feasibility for practical applications has been demonstrated with examples.

Acknowledgments

The authors are grateful to financial support by Roll-Royce Corp. through its internal research project. The first author (KW) also greatly appreciates Prof. Yunzhi Wang, Prof. J.E. Morral, and Dr. Ximiao Pan at The Ohio State University for valuable discussions.

References

1. A.A. Wheeler, W.J. Boettinger, and G.B. McFadden, Phase-Field Model for Isothermal Phase Transitions in Binary Alloys, *Phys. Rev. A*, 1992, **45**(10), p 7424-7439
2. J.A. Warren and W.J. Boettinger, Prediction of Dendritic Growth and Microsegregation Patterns in a Binary Alloy Using the Phase-Field Method, *Acta Metall. Mater.*, 1995, **43**(2), p 689-703
3. J. Tiaden, B. Nestler, H.J. Diepers, and I. Steinbach, The Multiphase-Field Model with an Integrated Concept for Modeling Solute Diffusion, *Phys. D*, 1998, **115**(1-2), p 73-86
4. G. Rubin and A.G. Khachaturyan, Three-Dimensional Model of Precipitation of Ordered Intermetallics, *Acta Mater.*, 1995, **47**(7), p 1995-2002
5. Y.H. Wen, Y. Wang, and L.Q. Chen, Phase-Field Simulation of Domain Structure Evolution During a Coherent Hexagonal-to-Orthorhombic Transformation, *Philos. Mag. A*, 2000, **80**(9), p 1967-1982
6. Y. Wang, L.Q. Chen, and A.G. Khachaturyan, Kinetics of Strain-Induced Morphological Transformation in Cubic Alloys with a Miscibility Gap, *Acta Metall. Mater.*, 1993, **41**(1), p 279-296

7. D.N. Fan, C.W. Geng, and L.Q. Chen, Computer Simulation of Topological Evolution in 2-D Grain Growth Using a Continuum Diffuse-Interface Field Model, *Acta Mater.*, 1997, **45**(3), p 1115-1126
8. A. Kazaryan, B.R. Patton, S.A. Dregia, and Y. Wang, On the Theory of Grain Growth in Systems with Anisotropic Boundary Mobility, *Acta Mater.*, 2002, **50**(3), p 499-510
9. A. Kazaryan, Y. Wang, S.A. Dregia, and B.R. Patton, Grain Growth in Anisotropic Systems: Comparison of Effect of Energy and Mobility, *Acta Mater.*, 2002, **50**(10), p 2491-2502
10. N. Ma, A. Kazaryan, S.A. Dregia, and Y. Wang, Computer Simulation of Texture Development During Grain Growth: Effect of Boundary Properties and Initial Microstructure, *Acta Mater.*, 2004, **41**(13), p 3869-3879
11. Y.U. Wang, Y.M. Jin, and A.G. Khachaturyan, Phase Field Microelasticity Modeling of Dislocation Dynamics Near Free Surface and in Heteroepitaxial Thin Films, *Acta Mater.*, 2003, **51**(14), p 4209-4223
12. C. Shen and Y. Wang, Phase Field Model of Dislocation Networks, *Acta Mater.*, 2003, **51**(9), p 2595-2610
13. C. Shen and Y. Wang, Incorporation of γ-Surface to Phase Field Model of Dislocations: Simulating Dissociation of Dislocations in F.C.C. Crystals, *Acta Mater.*, 2004, **52**(3), p 683-691
14. S.G. Kim, W.T. Kim, and T. Suzuki, Interfacial Compositions of Solid and Liquid in a Phase-Field Model with Finite Interface Thickness for Isothermal Solidification in Binary Alloys, *Phys. Rev. E*, 1998, **58**(3), p 3316-3323
15. S.G. Kim, W.T. Kim, and T. Suzuki, Phase-Field Model for Binary Alloys, *Phys. Rev. E*, 1999, **60**(6), p 7186-7197
16. S.G. Kim, A Phase-Field Model with Antitrapping Current for Multicomponent Alloys with Arbitrary Thermodynamic Properties, *Acta Mater.*, 2007, **55**(13), p 4391-4399
17. I. Steinbach, F. Pezzolla, B. Nestler, M. SeeBelberg, R. Prieler, G.J. Schmitz, and J.L.L. Rezende, A Phase Field Concept for Multiphase Systems, *Phys. D*, 1996, **94**(3), p 135-147
18. J.W. Cahn and J.E. Hilliard, Free Energy of a Nonuniform System. I. Interfacial Free Energy, *J. Chem. Phys.*, 1958, **28**(2), p 258-267
19. J.O. Andersson and J. Ågren, Models for Numerical Treatment of Multicomponent Diffusion in Simple Phases, *J. Appl. Phys.*, 1992, **72**(4), p 1350-1355
20. L.D. Landau and E.M. Lifshitz, *Statistical Physics*, Pergamon Press, Oxford, 1980
21. S.M. Allen and J.W. Cahn, A Microscopic Theory for Antiphase Boundary Motion and Its Application to Antiphase Domain Coarsening, *Acta Metall.*, 1979, **27**, p 1085-1095
22. N. Saunders and A.P. Miodownik, *Calphad (Calculation of Phase Diagrams): A Comprehensive Guide*, Elsevier Science Ltd., New York, 1998
23. A. Engström and J. Ågren, Assessment of Diffusional Mobilities in Face-Centered Cubic Ni-Cr-Al Alloys, *Z. Metallkd.*, 1996, **87**, p 92-97
24. C.E. Campbell, W.J. Boettinger, and U.R. Kattner, Development of a Diffusion Mobility Database for Ni-Base Superalloys, *Acta Mater.*, 2002, **50**(4), p 775-792
25. F. Zhang, S.L. Chen, F.Y. Xie, Y.A. Chang, W.A. Oates, and R. Schmid-Fetzer, Thermodynamic Databases: Useful Tools in the Development of Advanced Materials, *Advances in Materials Technology for Fossil Power Plants: Proceedings from the Fourth International Conference*, R. Viswanathan, D. Gandy, and K. Coleman, Ed. (Hilton Head Island, SC), ASM, 2004, p 1027-1041
26. B. Gleeson, W. Wang, S. Hayashi, and D.J. Sordelet, Effects of Platinum on the Interdiffusion and Oxidation Behavior of Ni-Al-Based Alloys, *Mater. Sci. Forum*, 2004, **461-464**, p 213-222
27. S. Hayashi, W. Wang, D.J. Sordelet, and B. Gleeson, Interdiffusion Behavior of Pt-Modified γ-Ni + γ′-Ni_3Al Alloys Coupled to Ni-Al-Based Alloys, *Metall. Mater. Trans. A*, 2005, **36**(7), p 1769-1775